applied sciences

MDPI

Article

Cauchy Norm-Constrained Nonstationary High-Resolution Processing for Seismic Data

Shengjun Li *, Jinyong Gui *, Bingyang Liu, Xin Guo and Hui Pan

Research Institute of Petroleum Exploration and Development, Northwest, Lanzhou 730020, China
* Correspondence: li_sj@petrochina.com.cn (S.L.); guijy@petrochina.com.cn (J.G.)

Abstract

Due to the intrinsic Q attenuation of geological formations, seismic waves experience amplitude and frequency attenuation during propagation, which results in reduced resolution and pronounced discrepancies between shallow and deep seismic data. Specifically, deep reflections exhibit weakened amplitudes and diminished high-frequency content. To mitigate these effects, a Q-compensation method based on nonstationary inversion is proposed to enhance seismic resolution and improve vertical consistency. A nonstationary reflectivity inversion framework is first established using a nonstationary convolution model with Cauchy norm regularization. The formation quality factor (Q) is then estimated from seismic data via the spectral ratio method using selected shallow and deep time windows. By incorporating the estimated Q value and an initial seismic wavelet, the proposed inversion simultaneously compensates for Q attenuation and wavelet effects, yielding a high-resolution reflectivity series. Q-compensated seismic data are subsequently reconstructed through the convolution of this reflectivity and an appropriate seismic wavelet. Both the model test and the field data application results demonstrate that the proposed method effectively compensates for Q attenuation, significantly enhances seismic resolution, and restores amplitude and frequency consistency between shallow and deep data.

Keywords: intrinsic Q-attenuation; shallow-to-deep consistency; seismic resolution; nonstationary inversion; Cauchy norm; Q-compensation

1. Introduction

With increasing exploration depth and structural complexity in hydrocarbon reservoirs, high-quality seismic data have become essential for reliable subsurface imaging and interpretation. A key factor degrading seismic data quality is intrinsic attenuation of formations, which causes seismic wave amplitude and frequency decay, as well as phase distortion during propagation. This attenuation is typically quantified by the quality factor Q. Q is a dimensionless parameter that quantifies the ratio of elastic energy stored in the formation to the energy lost per vibration cycle. A high Q value indicates weak attenuation and effective energy preservation, while a low Q value corresponds to strong energy loss and rapid spectral decay. As a consequence, Q attenuation (intrinsic attenuation) reduces seismic resolution and introduces pronounced amplitude and frequency discrepancies between shallow and deep reflections, thereby limiting interpretation accuracy in deeper targets. Numerous high-resolution seismic processing techniques have been developed to alleviate these effects, including deconvolution, inverse Q filtering, spectral whitening, time-frequency analysis, well-constrained frequency extension, and Q-migration imaging. Deconvolution improves seismic resolution by compressing the seismic wavelet, but

Check for updates

Academic Editor: Roberto Zivieri

Received: 27 November 2025
Revised: 2 February 2026
Accepted: 5 February 2026
Published: 22 April 2026

Copyright: © 2026 by the authors. Licensee MDPI, Basel, Switzerland. This article is an open access article distributed under the terms and conditions of the Creative Commons Attribution (CC BY) license.

generally relies on the assumption of a minimum-phase wavelet [1,2]. Inverse Q filtering compensates for attenuation-induced amplitude and phase distortions; however, amplitude compensation is often numerically unstable and prone to noise amplification, particularly in low signal-to-noise environments [3,4]. Spectral whitening assumes the reflectivity is white noise and improves seismic resolution by performing frequency band decomposition and equalization of seismic traces. It is convenient to operate but frequently compromises amplitude fidelity [5,6]. Time-frequency analysis methods (such as S-transform, wavelet transform, and Gabor transform) transform seismic data into the time-frequency domain for signal analysis. Different frequency extension techniques are then adopted to enhance seismic resolution [7,8]. However, these methods are prone to time-window truncation effects, resulting in unsatisfactory frequency extension outcomes. Well-constrained seismic frequency extension integrates multi-scale information from various geophysical data such as logging, cross-well seismic, and seismic data. Data matching inconsistencies among different sources may influence its application effectiveness [9,10]. Q migration incorporates attenuation compensation during imaging [11,12]. It mainly includes ray-theory Q migration, one-way wave equation Q migration, and two-way wave equation Q migration. Ray-theory Q migration features a straightforward algorithm. It is suitable for attenuation compensation and imaging in regions with simple geological structures, yet it neglects the dynamic properties of seismic waves [13,14]. Compared with ray-theory Q migration, one-way wave equation Q migration delivers higher precision in attenuation compensation. However, restricted by the one-way wave equation itself, this method still has limited performance in imaging and Q compensation for complex geological structures [15,16]. Two-way wave equation Q migration can further improves the performance of imaging and Q compensation [17,18]. In addition, nonstationary inversion is also a crucial approach for high-resolution seismic processing [19–23]. Inverse Q filtering often suffers from numerical instability during amplitude compensation. To address this issue, nonstationary inversion combines Q compensation with inversion. By introducing the Q-attenuation factor and solving the corresponding inversion equation, it simultaneously suppresses the impacts of Q filtering and seismic wavelet filtering, thus improving seismic resolution [24–28]. Since regularization constraints are added during the inversion process, this method can effectively avoid numerical instability associated with amplitude compensation.

To address the problem of low seismic resolution and inconsistent amplitude and frequency between shallow and deep data, this paper develops a nonstationary high-resolution processing method with Cauchy norm constraint. Firstly, we establish a nonstationary inversion constrained by Cauchy norm. Secondly, we extract time windows from shallow and deep seismic data and estimate the formation quality factor Q via the spectral ratio method. Thirdly, we obtain the seismic wavelet from the shallow data as the initial wavelet. Finally, the initial wavelet and the estimated Q value are then input into the nonstationary inversion for Q-compensated inverted reflectivity extraction. This reflectivity is then used to reconstruct the Q-compensated seismic data, which helps enhance seismic resolution and amplitude–frequency consistency.

2. Methodology

When seismic waves propagate in subsurface media, they are affected by the intrinsic attenuation of formations. This gives rise to amplitude attenuation, bandwidth reduction, and phase distortion. Such attenuation behavior is usually quantified by the quality factor Q. Traditional seismic inversion is mostly built upon the stationary convolution model

$$\mathbf{d} = \mathbf{G}\mathbf{r} \tag{1}$$

where **d** is the synthetic seismic record, **G** is the stationary wavelet matrix, and **r** is the reflectivity series, which refers to the reflection intensity of seismic waves at subsurface interfaces. It further reflects impedance contrasts and serves as a key input for synthetic record generation and seismic inversion. The reflectivity can be expressed as

$$r_j = \frac{v_{j+1}\rho_{j+1} - v_j\rho_j}{v_{j+1}\rho_{j+1} + v_j\rho_j} \quad j = 1,\ 2,\ \ldots,\ \mathrm{M}-1 \tag{2}$$

where r_j is an element of the reflectivity vector **r**, M is the number of sampling points in seismic data, and v_j and ρ_j are the formation velocity and density values at each sampling point, respectively. The product of velocity and density, $v_j\rho_j$, represents the formation impedance. In Equation (1), the seismic wave is assumed to be time-invariant (i.e., stationary). This means its energy, frequency, and phase remain unchanged during propagation. However, seismic waves are inevitably affected by intrinsic formation attenuation, also known as Q attenuation. With increasing propagation time, wave amplitude and frequency decline rapidly, accompanied by obvious phase distortion. This indicates that seismic waves are actually time-varying and nonstationary. In such situations, the convolution model adopted for time-variant wavelet synthetic seismograms is a nonstationary convolution model. Therefore, stationary inversion based on Equation (1) fails to resolve the inconsistency of resolution and amplitude between shallow and deep attenuated data. Its ability to enhance seismic resolution is therefore restricted. According to the Kjartansson Q-attenuation model, the formation attenuation factor $\alpha(\omega, \tau)$ [27] can be expressed as

$$\alpha(\omega,\tau) = e^{-i\omega\tau\left(\left(\frac{\omega}{\omega_0}\right)^{-\frac{1}{\pi Q(\tau)}} - \frac{i}{2Q(\tau)}\left(\frac{\omega}{\omega_0}\right)^{-\frac{1}{\pi Q(\tau)}} - 1\right)} = e^{-i\omega\tau\left(\left(\frac{\omega}{\omega_0}\right)^{-\frac{1}{\pi Q(\tau)}} - 1\right)} e^{\frac{-\omega\tau}{2Q(\tau)}\left(\frac{\omega}{\omega_0}\right)^{-\frac{1}{\pi Q(\tau)}}} \tag{3}$$

where ω is the angular frequency, τ is the seismic wave propagation time, e is the natural constant, i is the imaginary unit, ω_0 is the reference angular frequency, and $Q(\tau)$ is the quality factor at the formation location corresponding to the propagation time τ. By introducing the attenuation factor $\alpha(\omega, \tau)$ into the stationary convolution model, we establish the nonstationary convolution model

$$\mathbf{d} = \mathbf{G}(\mathbf{q})\mathbf{r} = \mathbf{F}^{-1}(\mathbf{WA})\mathbf{r}, \tag{4}$$

where $\mathbf{G}(\mathbf{q}) = \mathbf{F}^{-1}(\mathbf{WA})$ is the attenuated wavelet matrix that accounts for the influence of $\alpha(\omega, \tau)$, with **A** being its matrix form; $\mathbf{q} = [\mathrm{Q}_1, \mathrm{Q}_2, \ldots, \mathrm{Q}_\mathrm{M}]^T$ is the formation quality factor vector; T is the transpose symbol; and Q_j $(1 \le j \le \mathrm{M})$ is the quality factor value at each sampling point. **F** is the Fourier transform operator, which decomposes a signal into sinusoidal components and yields its global frequency-domain representation; $\mathbf{F}^{-1}$ is the inverse Fourier transform operator; and **W** is the matrix form of the frequency-domain initial seismic wavelet $\mathrm{W}(\omega)$. Obviously, when attenuation is zero (i.e., Q value is infinite), the attenuation factor is 1, that is,

$$\lim_{Q(\tau)\to\infty} \alpha(\omega,\tau) = \lim_{Q(\tau)\to\infty} e^{-i\omega\tau\left(\left(\frac{\omega}{\omega_0}\right)^{-\frac{1}{\pi Q(\tau)}} - 1\right)} e^{\frac{-\omega\tau}{2Q(\tau)}\left(\frac{\omega}{\omega_0}\right)^{-\frac{1}{\pi Q(\tau)}}} = 1. \tag{5}$$

Then, the nonstationary convolution model shown in Equation (4) degenerates into the stationary convolution model

$$\mathbf{d} = \mathbf{F}^{-1}(\mathbf{W})\mathbf{r}, \tag{6}$$

where $\mathbf{F}^{-1}(\mathbf{W})$ is equivalent to the matrix $\mathbf{G}$ in Equation (1). The nonstationary convolution model in Equation (4) is used to synthesize attenuated seismic records. In practical applications, discrepancies always exist between the synthetic records and the observed records acquired by the geophone, denoted as $\mathbf{d}^{obs}$. The error between them can be quantified using the sum of squared errors

$$O(\mathbf{r}) = \left\| \mathbf{d}^{obs} - \mathbf{G}(\mathbf{q})\mathbf{r} \right\|_2^2 \tag{7}$$

Based on the sparse assumption of the formation, we introduce a sparse regularization term constrained by Cauchy norm. Equation (7) is then rewritten as

$$O(\mathbf{r}) = \left\| \mathbf{d}^{obs} - \mathbf{G}(\mathbf{q})\mathbf{r} \right\|_2^2 + \lambda \sum_{j=1}^{\mathrm{M}} \ln\left(1 + \frac{r_j^2}{2}\right), \tag{8}$$

where λ is the sparse constraint factor, and r_j $(1 \le j \le \mathrm{M})$ is the element of the reflectivity series $\mathbf{r}$. In practice, obtaining the Q value at every sampling point for Q compensation is impractical. Instead, an equivalent Q value can be estimated to characterize the formation attenuation. Under this condition, Equation (8) is revised to

$$O(\mathbf{r}) = \left\| \mathbf{d}^{obs} - \mathbf{G}\left(Q_{eff}\right)\mathbf{r} \right\|_2^2 + \lambda \sum_{j=1}^{\mathrm{M}} \ln\left(1 + \frac{r_j^2}{2}\right), \tag{9}$$

where Q_{eff} is the equivalent Q value of the formation. By differentiating Equation (9) with respect to the reflectivity $\mathbf{r}$ and setting the derivative to $\mathbf{0}$, we obtain

$$\mathbf{G}\left(Q_{eff}\right)^T \mathbf{G}(Q_{eff})\mathbf{r} + \lambda \sum_{j=1}^{\mathrm{M}} \left(\frac{2r_j}{r_j^2 + 2}\right) = \mathbf{G}\left(Q_{eff}\right)^T \mathbf{d}^{obs}, \tag{10}$$

which can be further expressed as

$$\mathbf{r} = \left[\mathbf{G}\left(Q_{eff}\right)^T \mathbf{G}(Q_{eff}) + \lambda \cdot Diag\left(\frac{2}{r_1^2 + 2}, \frac{2}{r_2^2 + 2}, \ldots, \frac{2}{r_{\mathrm{M}}^2 + 2}\right)\right]^{-1} \mathbf{G}\left(Q_{eff}\right)^T \mathbf{d}^{obs} \tag{11}$$

In Equation (11), *Diag* denotes a diagonal matrix. Since the reflectivity appears on both sides of Equation (11), the equation cannot be solved directly. In this paper, the iterative reweighted algorithm is adopted to solve Equation (11). After obtaining the reflectivity, an appropriate seismic wavelet $\mathbf{w}$ is selected to reconstruct the high-resolution seismic data

$$\mathbf{S} = \mathbf{w}^* \mathbf{r}. \tag{12}$$

The final high-resolution seismic data show significantly improved resolution in the middle and deep layers and higher vertical frequency–amplitude consistency. It thus provides a more reliable foundation for geological interpretation of middle and deep formations.

3. Model and Field Data Tests

3.1. Model Test

In the model test section, the Marmousi reflectivity model is adopted to verify the effectiveness of the proposed method. Figure 1a shows the Marmousi reflectivity model. Figure 1b is the synthetic attenuation-free seismic record using the reflectivity model, with a Ricker wavelet with a 50 Hz dominant frequency. The amplitude spectrum comparison between deep (1400–1500 ms) and shallow (0–100 ms) attenuation-free seismic records reveals high consistency (Figure 1c). The dominant frequency remains stable at approxi-

mately 50 Hz. Based on Equation (4), a nonstationary seismic record is synthesized using the same reflectivity model, followed by the addition of 5% random noise (Figure 1d). The initial seismic wavelet used is the 50 Hz dominant-frequency Ricker wavelet, and the equivalent Q value is set to 50. When formation attenuation is present, the energy of the deep seismic record is significantly weakened, and the dominant frequency shifts to lower frequencies (Figure 1e). Figure 1f shows the seismic wavelet extracted from the entire attenuated seismic record (0–1500 ms). This extracted wavelet is used for stationary sparse inversion. The initial wavelet and inverted reflectivity are then convolved to reconstruct the seismic record (Figure 2a). Since the Q-attenuation effect of the formation is not considered, the reconstructed seismic record still shows weak reflection energy and low frequency in the deep part (Figure 2b). The amplitude–frequency consistency between shallow and deep records is not improved. Therefore, it is necessary to further account for nonstationary inversion to compensate for formation Q attenuation and to improve seismic resolution.

To compensate for Q attenuation, the Q value is first estimated using the spectral ratio method. Figure 2d shows the fitting curve when calculating the Q value using the spectral ratio method. Using the effective frequency band of 0–45 Hz for linear fitting, the estimated quality factor is 56.8738. This estimated Q value and the initial seismic wavelet are input into the nonstationary inversion process based on Equation (11). Using Equation (12), the inverted reflectivity from nonstationary inversion is convolved with the initial wavelet to generate the reconstructed seismic record (Figure 2e). As Q-attenuation effects are considered, the reconstructed seismic record achieves a marked improvement in amplitude and frequency consistency between shallow and deep parts (Figure 2f). A comparison of the amplitude spectra of the attenuation-free, attenuated, and reconstructed seismic records (Figure 2g) shows that the spectrum characteristics of the reconstructed record are close to those of the attenuation-free record. However, since the estimated Q value is slightly larger than the true value, the energy of the reconstructed record is marginally lower than that of the attenuation-free record. Calculation of the correlation coefficient between the attenuation-free and reconstructed seismic records shows their correlation reaches 93.74%. Although the slight overestimation of the Q value leads to minor undercompensation, the high correlation coefficient further confirms the accuracy and validity of the Q compensation in this case. Nevertheless, compared with the record reconstructed by stationary inversion, nonstationary inversion significantly enhances both the resolution of the seismic record and the consistency between shallow and deep parts.

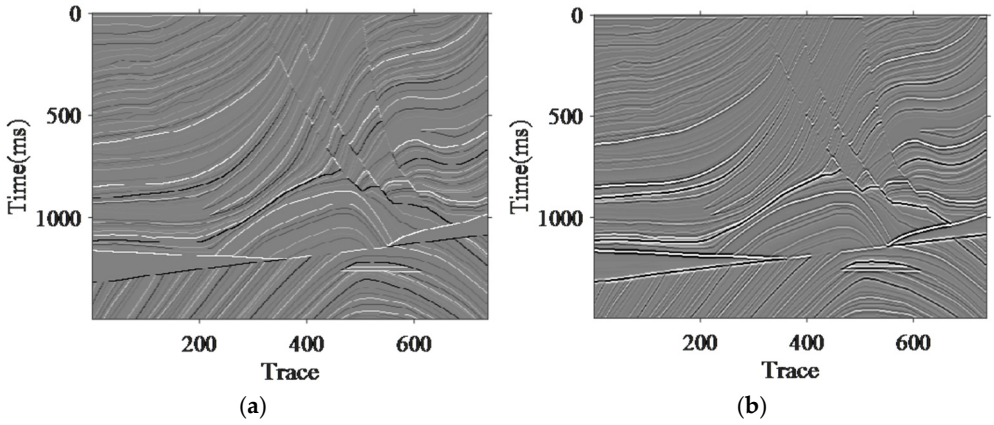


Figure 1. *Cont.*

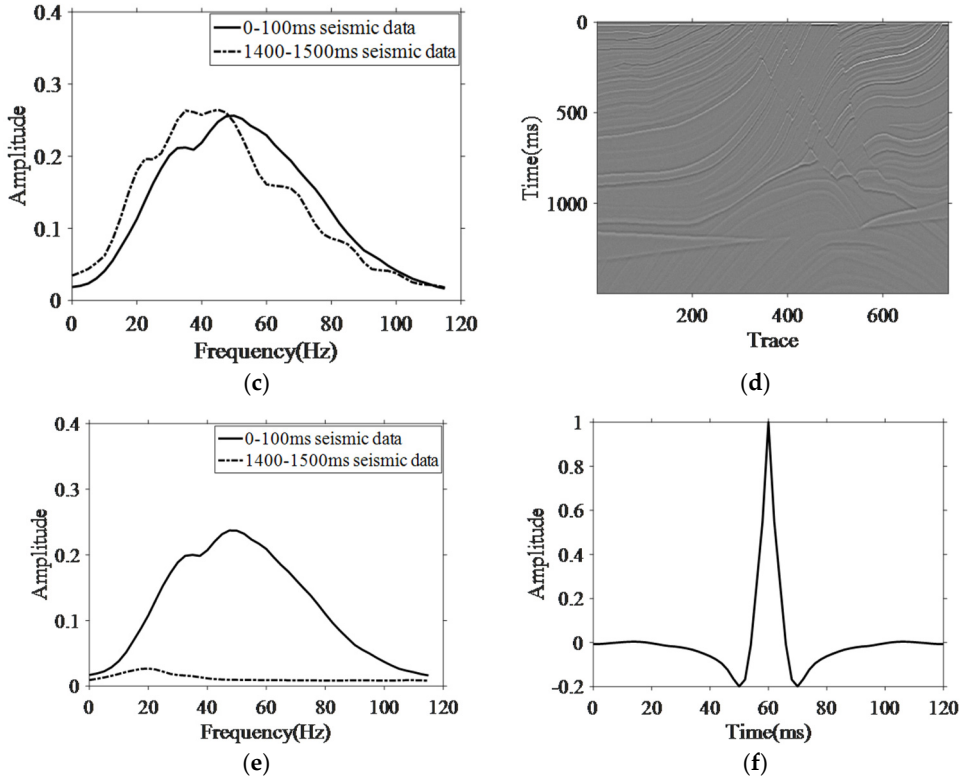


Figure 1. The Marmousi model experiment: (**a**) Marmousi reflectivity model. The horizontal axis represents the seismic traces, each of which refers to a time-series record of a seismic signal or reflectivity. (**b**) Synthetic attenuation-free seismic data. (**c**) The amplitude spectrum comparison between the shallow and deep attenuation-free seismic data. (**d**) Synthetic attenuated seismic data (with 5% random noise). (**e**) The amplitude spectrum comparison between the shallow and deep attenuated seismic data. (**f**) The seismic wavelet extracted from synthetic attenuated seismic data.

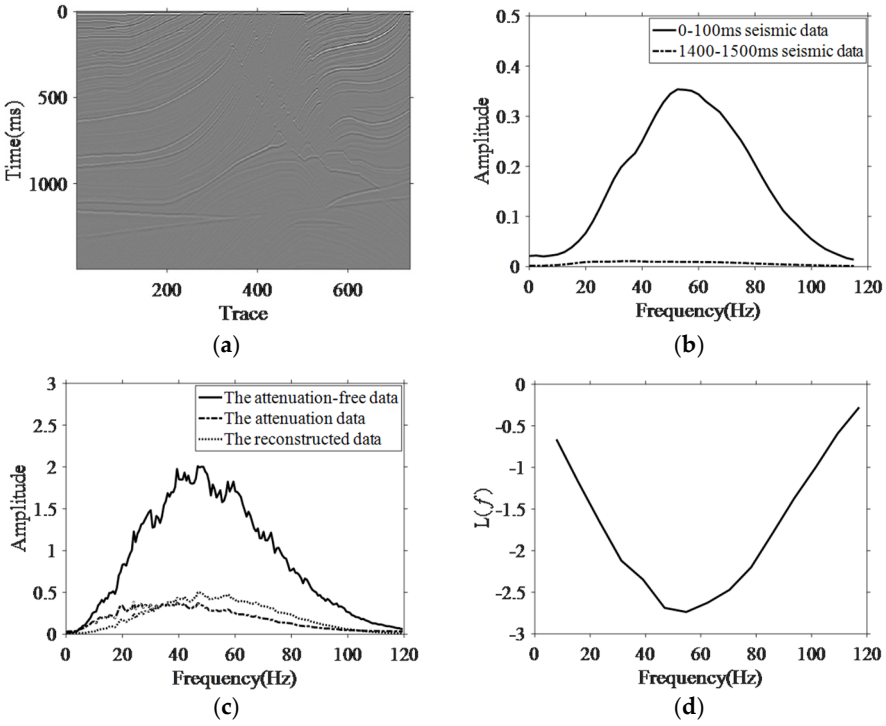


Figure 2. *Cont.*

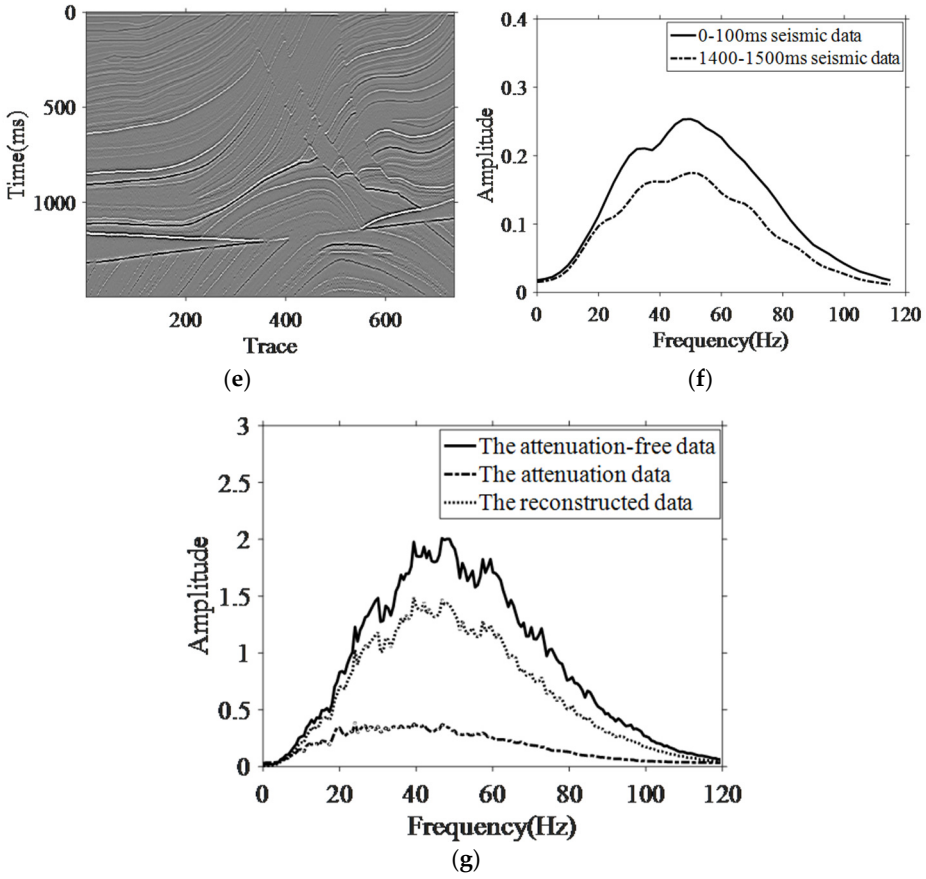


Figure 2. The processing results of Marmousi model experiment: (**a**) Reconstructed seismic data obtained by using stationary inversion, where the wavelet used for stationary inversion is the seismic wavelet shown in Figure 1f, and the wavelet used for reconstructing seismic data is the initial seismic wavelet. (**b**) Amplitude spectrum comparison between the shallow and deep parts of reconstructed seismic data in (**a**). (**c**) The amplitude spectrum comparison among the attenuation-free seismic data in Figure 1b, the attenuated seismic data in Figure 1d and the reconstructed seismic profile in (**a**). (**d**) The fitted curve when using the spectral ratio method to calculate Q from attenuated seismic data. The selected effective frequency band is 0–45 Hz, and the estimated Q value is 56.8738. (**e**) The seismic data reconstructed using nonstationary inversion with an equivalent Q value of 56.8738. The wavelets used for nonstationary inversion and for reconstructing the seismic data are both the initial seismic wavelet. (**f**) The amplitude spectrum comparison between the shallow and deep reconstructed seismic data of (**e**). (**g**) The amplitude spectrum comparison between the attenuation-free seismic data in Figure 1b, the attenuated seismic data in Figure 1d and the reconstructed seismic profile in (**e**).

3.2. Field Data Test

To further verify the proposed method's effectiveness, we apply it to field seismic data. Figure 3a presents the original seismic data, which exhibit obvious attenuation. Compared with shallow seismic data, deep data have weaker energy, lower resolution, and coarser reflection events. Comparative analysis of amplitude spectra for shallow (0–100 ms) and deep (900–1000 ms) data reveals significant attenuation in the deep part. The dominant frequency drops from approximately 50 Hz in the shallow part to around 25 Hz, and the amplitude value is reduced by roughly half (Figure 3b). We extracted seismic wavelets from the shallow part (1–100 ms) and the entire original data volume using the autocorrelation method (Figure 3c,d), respectively. The wavelet shown in Figure 3c is used as the initial seismic wavelet. First, we performed stationary inversion on the original seismic data with the wavelet shown in Figure 3d. Next, the wavelet shown in Figure 3c was convolved with the inverted reflectivity to reconstruct the seismic data (Figure 4a).

Since no Q compensation was applied in this process, the deep part of the reconstructed seismic data still showed obvious low-frequency and weak-amplitude characteristics. The amplitude spectrum comparison between the shallow and deep parts indicates persistent significant differences in resolution and energy distribution. Deep data attenuation remains uncompensated. To address this issue, we used the nonstationary high-resolution method to process the field seismic data. Based on the spectral ratio method, we conducted linear fitting within the 5–100 Hz effective frequency band (Figure 4d), yielding an estimated Q value of 95.8824. This Q value and the initial seismic wavelet (Figure 3c) were substituted into Equation (11). Using the iteratively reweighted algorithm, we solved the nonstationary inversion equation to obtain the inverted reflectivity series. The Q-compensated seismic data (Figure 4e) were achieved by convolving the nonstationarily inverted reflectivity with the initial seismic wavelet. After nonstationary inversion compensation, the reconstructed seismic data showed marked improvements (Figure 4g). The energy of deep seismic data was effectively restored, and the amplitude and frequency distribution of shallow and deep data became more consistent (Figure 4f). The dominant frequency of deep data increased from about 25 Hz to roughly 50 Hz. Structural details in the seismic profile were clearer, especially in the deep areas where blurred reflection features were now distinguishable. These improvements fully confirm the method's ability to enhance seismic resolution and maintain amplitude fidelity, providing reliable data support for subsequent structural interpretation and reservoir prediction.

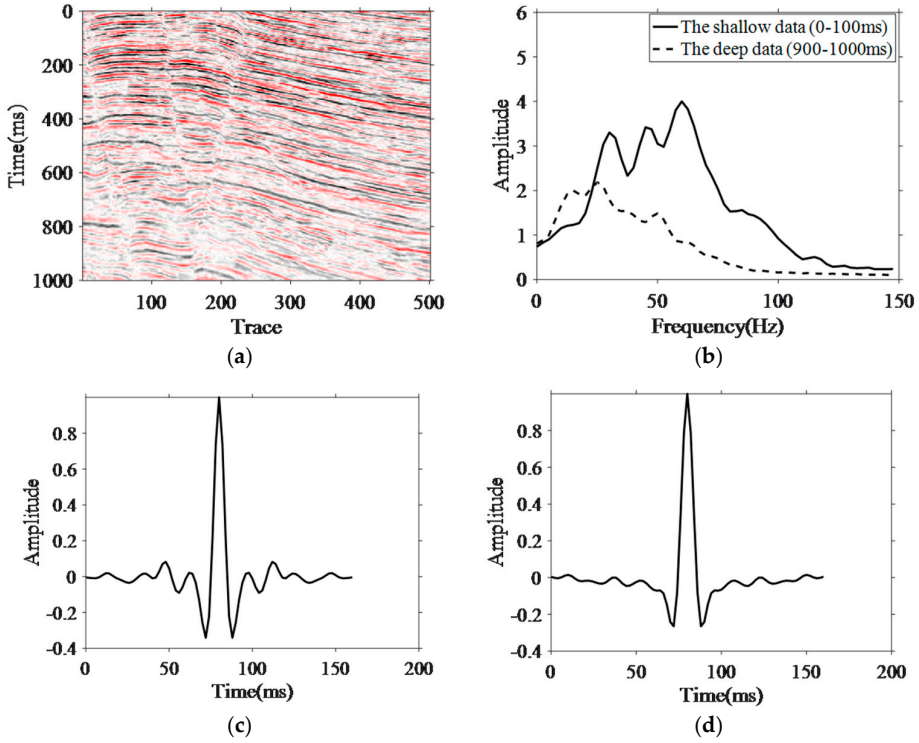


Figure 3. The field seismic data experiment: (**a**) The original seismic data. (**b**) The amplitude spectra of the original shallow (0–100 ms) and deep (900–1000 ms) seismic data in (**a**). (**c**) The initial seismic wavelet extracted from the original shallow (0–100 ms) seismic data. (**d**) The seismic wavelet extracted from the whole original seismic data.

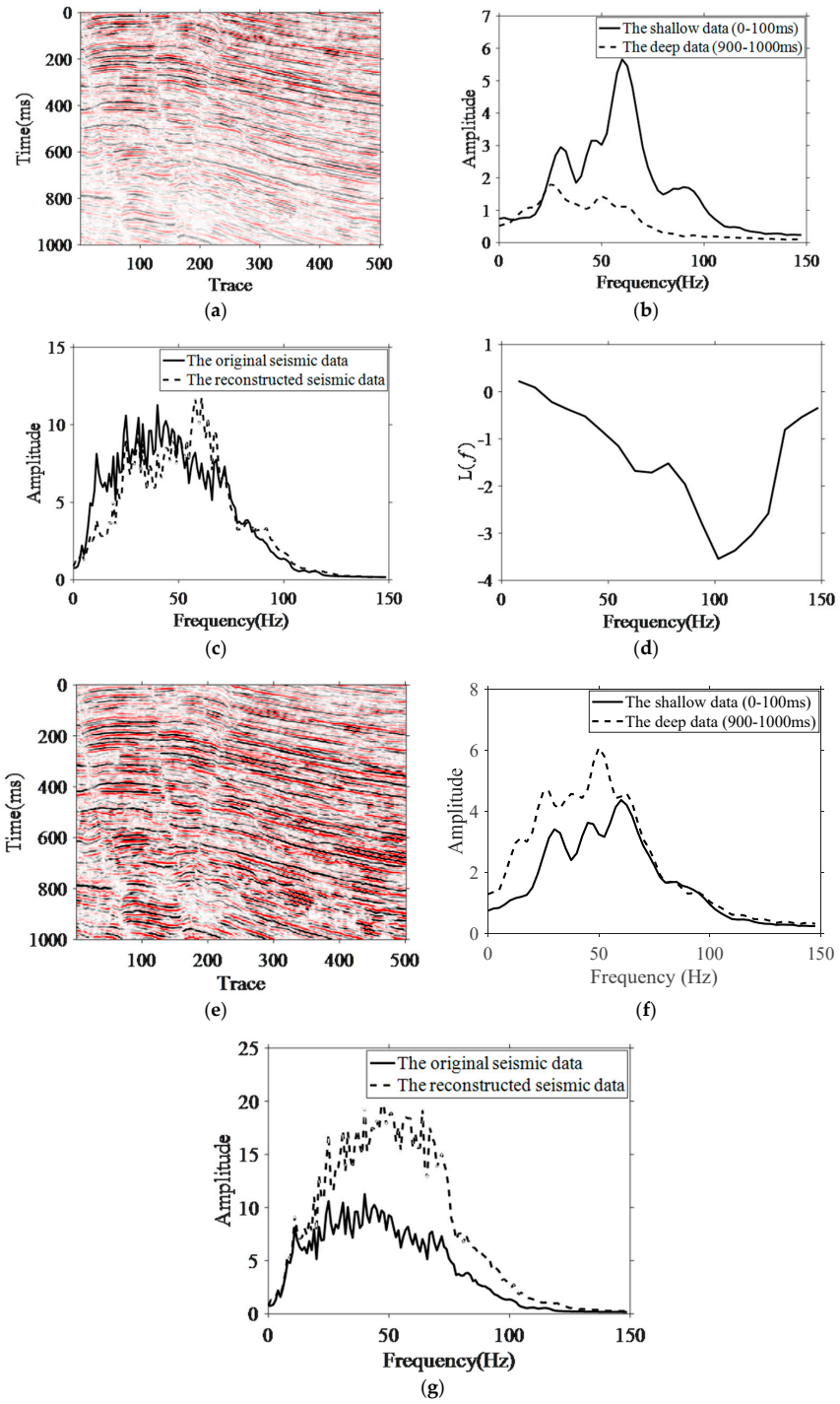


Figure 4. The processing results of the field data experiment: (**a**) The reconstructed seismic data obtained by using stationary inversion, where the wavelet used for stationary inversion is the seismic wavelet shown in Figure 3d, and the wavelet used for reconstructing seismic data is the initial seismic wavelet in Figure 3c. (**b**) The amplitude spectrum comparison between the shallow and deep parts of reconstructed seismic data from (**a**). (**c**) The amplitude spectrum comparison between the original seismic data in Figure 3a and the reconstructed seismic data in (**a**). (**d**) The fitted curve when using the spectral ratio method to calculate Q from the original seismic data. The selected effective frequency band is 5–100 Hz, and the estimated Q value is 95.8824. (**e**) The seismic data reconstructed using nonstationary inversion with an equivalent Q value of 95.8824. The wavelets used for nonstationary inversion and for reconstructing the seismic data are both the initial seismic wavelet in Figure 3c. (**f**) The amplitude spectrum comparison between the shallow and deep parts of reconstructed seismic data of (**e**). (**g**) The amplitude spectrum comparison between the original seismic data in Figure 3a and the reconstructed seismic data in (**e**).

4. Discussion

This study confirms that the Cauchy norm-constrained nonstationary method effectively compensates for Q attenuation. It outperforms stationary inversion. The Cauchy norm constraint balances sparsity and amplitude fidelity. It avoids noise amplification and over-sparsification, thereby improving shallow-to-deep consistency. Q estimation accuracy—dependent on the spectral ratio method—directly affects compensation effects. Minor Q deviations can cause undercompensation or overcompensation. The constraint factor λ is selected manually, limiting automation. Future work will focus on improving spatiotemporal resolution of Q estimation, automating λ selection, and optimizing algorithm efficiency. This will adapt the method to 3D seismic data, expanding its application in complex exploration scenarios.

5. Conclusions

Based on the formation intrinsic Q-attenuation mechanism and inversion theory, this paper develops a nonstationary inversion method under Cauchy norm constraints. The goal is to achieve Q compensation through seismic data reconstruction. The method first estimates the Q value through the spectral ratio method. It then uses this Q value and the extracted initial seismic wavelet as inputs for nonstationary inversion. This process simultaneously eliminates wavelet and Q filtering effects to obtain Q-compensated inverted reflectivity. Subsequently, the initial seismic wavelet is convolved with the inverted reflectivity to reconstruct the seismic data. This improves seismic resolution and shallow-to-deep consistency. Both model data and field data processing validate the method's effectiveness and help to obtain the following conclusions:

1. The nonstationary high-resolution processing method in this paper effectively compensates for seismic wave energy and frequency losses caused by Q attenuation. It enhances seismic resolution, amplitude fidelity, and shallow-to-deep consistency.
2. This method has some limitations. It requires prior Q information and lacks independent Q-estimation capabilities. Insufficient Q-estimation accuracy directly impairs compensation effects. Future research should explore reasonable Q model estimation and efficient, stable nonstationary high-resolution processing without prior Q information.

Author Contributions: Conceptualization, S.L.; methodology, S.L. and J.G.; investigation, X.G.; data curation, B.L.; supervision, H.P. All authors have read and agreed to the published version of the manuscript.

Funding: This work was supported in part by the Prospective, Basic, and Strategic Technology Research Project of PetroChina (2021DJ0606), and Gansu Science and Technology Program (23ZDGA004).

Institutional Review Board Statement: Not applicable.

Informed Consent Statement: Not applicable.

Data Availability Statement: The data presented in this study are available on request from the corresponding authors.

Conflicts of Interest: The authors declare no conflict of interest.

References

1. Wang, L.; Zhao, Q.; Gao, J.; Xu, Z.; Fehler, M.; Jiang, X. Seismic sparse-spike deconvolution via Toeplitz-sparse matrix factorization. *Geophysics* **2016**, *8*, V169–V182. [CrossRef]
2. Wang, L.; Zhou, H.; Wang, Y.; Yu, B.; Fang, J. Adaptive seismic single channel deconvolution via convolutional sparse coding model. *IEEE Geosci. Remote Sens. Lett.* **2020**, *17*, 1415–1419. [CrossRef]
3. Wang, Y.H. A stable and efficient approach of inverse Q filtering. *Geophysics* **2002**, *67*, 657–663. [CrossRef]

4. Chai, X.; Wang, S.; Yuan, S.; Zhao, J.; Sun, L.; Wei, X. Sparse reflectivity inversion for nonstationary seismic data. *Geophysics* **2014**, *79*, V93–V105. [CrossRef]
5. Zheng, S.L. Whitening processing of seismic signal spectrum based on SSGST. *Int. J. Comput. Appl. Technol. Res.* **2020**, *9*, 130–132. [CrossRef]
6. Naskar, T.; Bhaumik, M.; Mukherjee, S.; Adari, S.V. Spectral whitening based seismic data preprocessing technique to improve the quality of surface wave's velocity spectra. *Comput. Geosci.* **2025**, *195*, 105784. [CrossRef]
7. Wang, Q.; Gao, J.; Liu, N.; Jiang, X. High-resolution seismic time-frequency analysis using the synchrosqueezing generalized S-transform. *IEEE Geosci. Remote Sens. Lett.* **2018**, *15*, 374–378. [CrossRef]
8. Zoukaneri, I.; Porsani, M.J. A combined Wigner-Ville and maximum entropy method for high-resolution time-frequency analysis of seismic data. *Geophysics* **2015**, *80*, O1–O11. [CrossRef]
9. Wang, Y.; Ge, Q.; Lu, W.; Yan, X. Well-logging constrained seismic inversion based on closed-loop convolutional neural network. *IEEE Trans. Geosci. Remote Sens.* **2020**, *58*, 5564–5574. [CrossRef]
10. Wu, D.K.; Wu, Z.W.; Wu, Y.J. A new method for high resolution well-control processing of post-stack seismic data. *Nat. Gas Ind. B* **2020**, *7*, 215–223. [CrossRef]
11. Bai, M.; Chen, X.; Wu, J.; Liu, G.; Chen, Y.; Chen, H.; Li, Q. Q-compensated migration by Gaussian beam summation method. *J. Geophys. Eng.* **2016**, *13*, 35–48. [CrossRef]
12. Xu, W.; Liu, H.-X.; Mi, H.-G.; Zhang, B.; Guo, J.-C.; Ge, Y.; You, J. High-precision Q modeling and Q migration technology and its applications in loess plateau regions. *Appl. Geophys.* **2024**, *21*, 835–847. [CrossRef]
13. Ribodetti, A.; Virieux, J. Asymptotic theory for imaging the attenuation factor Q. *Geophysics* **1998**, *63*, 1767–1778. [CrossRef]
14. Bai, M.; Chen, X.-H.; Wu, J.; Chen, Y.-K.; Liu, G.-C.; Wang, E.-J. Multiple-component Gaussian beam reverse-time migration based on attenuation compensation. *Chin. J. Geophys.* **2016**, *59*, 3379–3393. (In Chinese) [CrossRef]
15. Zhang, J.; Wapenaar, K. Wavefield extrapolation and prestack depth migration in anelastic inhomogeneous media. *Geophys. Prospect.* **2002**, *50*, 629–643. [CrossRef]
16. Guddati, M.N. Arbitrarily wide-angle wave equations for complex media. *Comput. Methods Appl. Mech. Eng.* **2006**, *195*, 65–93. [CrossRef]
17. Mulder, W.A.; Plessix, R.-E. A comparison between one-way and two-way wave-equation migration. *Geophysics* **2004**, *69*, 1491–1504. [CrossRef]
18. Dutta, G.; Schuster, G.T. Attenuation compensation for least-squares reverse time migration using the viscoacoustic-wave equation. *Geophysics* **2014**, *79*, S251–S262. [CrossRef]
19. Jiang, Y.; Cao, S.; Chen, S.; Wang, H.; Dai, H.; Li, X.; Zheng, D. Time-varying wavelet estimation and deconvolution for nonstationary data based on a FWE function. *J. Appl. Geophys.* **2020**, *183*, 104198. [CrossRef]
20. Cheng, L.; Yuan, S.Y.; Wang, S.X. Joint reflectivity and structural interval-Q estimation by using nonstationary sparse inversion. *IEEE Geosci. Remote Sens. Lett.* **2021**, *18*, 776–780. [CrossRef]
21. Yang, W.-Y.; Wang, W.; Li, G.-F.; Wei, X.-J.; Wang, W.-L.; Chen, D.-W. Nonstationary signal inversion based on shaping regularization for random noise attenuation. *Appl. Geophys.* **2020**, *17*, 432–442. [CrossRef]
22. Jamali, J.; Javaherian, A.; Wang, Y.; Ameri, M.J. Non-stationary inversion of seismic data for fracture compliances in azimuthally anisotropic media. *Pet. Geosci.* **2024**, *30*, petgeo2023-151. [CrossRef]
23. Sun, Y.; Cao, S.; Su, Y.; Zhou, J.; Ma, Z. Non-stationary multichannel spectral inversion of seismic data. *Stud. Geophys. Geod.* **2025**, *69*, 41–56. [CrossRef]
24. Chen, S.; Li, S.; Ma, Q.; Qin, L.; Yuan, S. An Optimally Oriented Coherence Attribute Method and Its Application to Faults and Fracture Sets Detection in Carbonate Reservoirs. *Appl. Sci.* **2025**, *15*, 7393. [CrossRef]
25. Li, S.; Gao, J.; Lou, Y.; Gui, J.; He, D.; Chang, D. Separation and suppression of strong reflections via a multiscale attention deep learning model. *IEEE Trans. Geosci. Remote Sens.* **2024**, *62*, 4504412. [CrossRef]
26. Li, F.; Wang, S.; Chen, X.; Liu, G.; Zheng, Q. A novel nonstationary deconvolution method based on spectral modeling and variable-step sampling hyperbolic smoothing. *J. Appl. Geophys.* **2014**, *103*, 132–139. [CrossRef]
27. Lari, H.H.; Gholami, A. Nonstationary blind deconvolution of seismic records. *Geophysics* **2019**, *84*, V1–V9. [CrossRef]
28. Cheng, L.; Chen, M.; Zhang, Z.; Liao, J.; Xu, C.; Li, A. Q estimation and compensation for attenuated seismic data with the scanning-Q nonstationary sparse inversion method. *Geophysics* **2025**, *90*, R275–R284. [CrossRef]

Disclaimer/Publisher's Note: The statements, opinions and data contained in all publications are solely those of the individual author(s) and contributor(s) and not of MDPI and/or the editor(s). MDPI and/or the editor(s) disclaim responsibility for any injury to people or property resulting from any ideas, methods, instructions or products referred to in the content.